

Synchronized cycles of bacterial lysis for *in vivo* delivery

M. Omar Din^{1*}, Tal Danino^{2†*}, Arthur Prindle¹, Matt Skalak², Jangir Selimkhanov¹, Kaitlin Allen², Ellixis Julio¹, Eta Atolia², Lev S. Tsimring³, Sangeeta N. Bhatia^{2,4,5,6,7,8§} & Jeff Hasty^{1,3,9§}

The widespread view of bacteria as strictly pathogenic has given way to an appreciation of the prevalence of some beneficial microbes within the human body^{1–3}. It is perhaps inevitable that some bacteria would evolve to preferentially grow in environments that harbour disease and thus provide a natural platform for the development of engineered therapies^{4–6}. Such therapies could benefit from bacteria that are programmed to limit bacterial growth while continually producing and releasing cytotoxic agents *in situ*^{7–10}. Here we engineer a clinically relevant bacterium to lyse synchronously at a threshold population density and to release genetically encoded cargo. Following quorum lysis, a small number of surviving bacteria reseed the growing population, thus leading to pulsatile delivery cycles. We used microfluidic devices to characterize the engineered lysis strain and we demonstrate its potential as a drug delivery platform via co-culture with human cancer cells *in vitro*. As a proof of principle, we tracked the bacterial population dynamics in ectopic syngeneic colorectal tumours in mice via a luminescent reporter. The lysis strain exhibits pulsatile population dynamics *in vivo*, with mean bacterial luminescence that remained two orders of magnitude lower than an unmodified strain. Finally, guided by previous findings that certain bacteria can enhance the efficacy of standard therapies¹¹, we orally administered the lysis strain alone or in combination with a clinical chemotherapeutic to a syngeneic mouse transplantation model of hepatic colorectal metastases. We found that the combination of both circuit-engineered bacteria and chemotherapy leads to a notable reduction of tumour activity along with a marked survival benefit over either therapy alone. Our approach establishes a methodology for leveraging the tools of synthetic biology to exploit the natural propensity for certain bacteria to colonize disease sites.

In order to control population levels and facilitate drug delivery using bacteria, we engineered a synchronized lysis circuit (SLC) using coupled positive and negative feedback loops that have previously been used to generate robust oscillatory dynamics^{12,13}. The circuit (Fig. 1a) consists of a common promoter that drives expression of both its own activator (positive feedback) and a lysis gene (negative feedback). Specifically, the *luxI* promoter regulates production of autoinducer (AHL), which binds LuxR and enables it to transcriptionally activate the promoter. Negative feedback arises from cell death that is triggered by a bacteriophage lysis gene (φ X174E) which is also under control of the *luxI* promoter^{13–15}. AHL can diffuse to neighbouring cells and thus provides an intercellular synchronization mechanism.

The bacterial population dynamics arising from the synchronized lysis circuit can be conceptualized as a slow build-up of the signalling

molecule (AHL) to a threshold level, followed by a lysis event that rapidly prunes the population and enables the release of bacterial contents (Fig. 1b). After lysis, a small number of remaining bacteria begin to produce AHL anew, allowing the ‘integrate and fire’ process to be repeated in a cyclical fashion. We used microfluidic devices to observe growth and lysis with the fluorescent protein superfolder GFP (sfGFP) as a proxy for circuit dynamics in attenuated *Salmonella enterica* subsp. *enterica* serovar Typhimurium (Supplementary Videos 1 and 2). We observed periodic lysis events characterized by peaks in the fluorescent reporter expression that correspond to population lysis (Fig. 1c). The fraction of lysed cells remains consistent across subsequent cycles, suggesting that lysis and survival occur in a stochastic manner (Extended

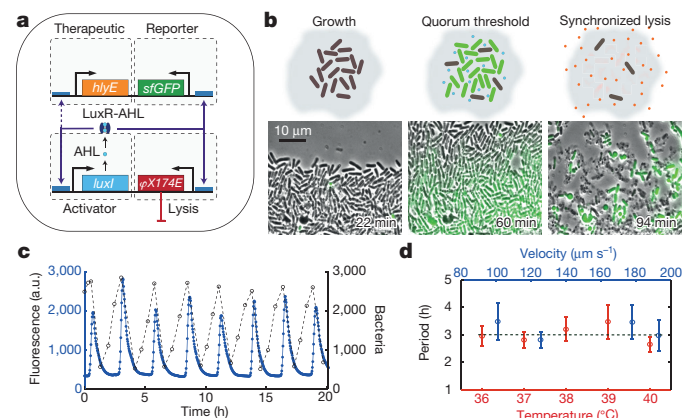


Figure 1 | Construction and characterization of the SLC. **a**, The circuit contains an activator¹³ and lysis plasmid. When the population reaches the quorum threshold at a critical AHL concentration, the *luxI* promoter drives the transcription of gene *E* for lysis, *luxI*, and *sfGFP* or *luxCDABE* as the reporter module. The *luxI* or the *tac* promoter also drives the transcription of the therapeutic gene for the stabilized circuit used *in vivo*. LuxR in this system is driven by the native *luxR* promoter. **b**, The main stages of each lysis cycle from seeding to quorum ‘firing’. Shown below the schematic depictions are typical time series images of the circuit-harboring cells undergoing the three main stages of quorum firing in a microfluidic growth chamber¹². **c**, Fluorescence profile of a typical microfluidic experiment. The estimated cell population trajectory reveals that lysis events correspond to peaks of sfGFP fluorescence. **d**, Period as a function of estimated flow velocity in the media channel of the microfluidic device and environmental temperature. Error bars indicate ± 1 s.d. for 13–50 peaks. These experiments were performed with strain 1, see Supplementary Information for complete strain information.

¹Department of Bioengineering, University of California, San Diego, La Jolla, California 92093, USA. ²Institute for Medical Engineering & Science, Massachusetts Institute of Technology, Cambridge, Massachusetts 02139, USA. ³BioCircuits Institute, University of California, San Diego, La Jolla, California 92093, USA. ⁴Broad Institute of Harvard and MIT, Cambridge, Massachusetts 02139, USA. ⁵Department of Medicine, Brigham and Women’s Hospital, Boston, Massachusetts 02139, USA. ⁶Electrical Engineering and Computer Science and David H. Koch Institute for Integrative Cancer Research, Massachusetts Institute of Technology, Cambridge, Massachusetts 02139, USA. ⁷Marble Center for Cancer Nanomedicine and Ludwig Center for Molecular Oncology, Massachusetts Institute of Technology, Cambridge, Massachusetts 02139, USA. ⁸Howard Hughes Medical Institute, Chevy Chase, Maryland 20815, USA. ⁹Molecular Biology Section, Division of Biological Science, University of California, San Diego, La Jolla, California 92093, USA. †Present address: Department of Biomedical Engineering, Columbia University, New York, New York 10027, USA.

*These authors contributed equally to this work.

§These authors jointly supervised this work.

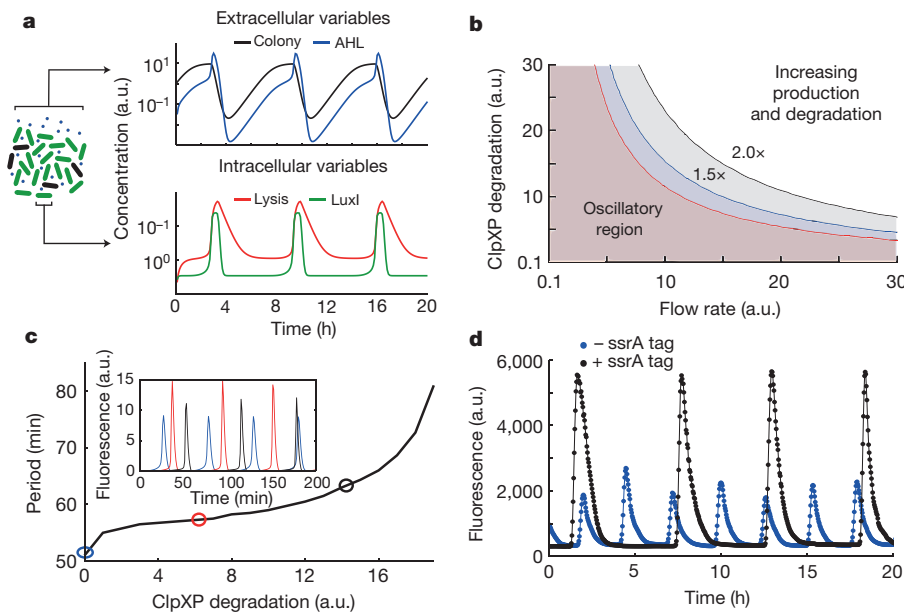


Figure 2 | Computational modelling and tunability. **a**, The model consists of intracellular variables (lysis protein E and LuxI concentrations) and extracellular variables (colony size and AHL concentrations). A time series of colony size (black), colony AHL (blue), intracellular LuxI (green) and lysis protein concentrations (red) are shown on the right. **b**, The region in the model parameter space for ClpXP-mediated degradation (see Supplementary Information) and flow where the model output is oscillatory increases with higher production and degradation terms. **c**, Results from the computational model showing the ability to tune the oscillatory period by varying ClpXP mediated degradation of LuxI. **d**, Fluorescence profiles showing lysis oscillations for LuxI *ssrA* (black, strain 2) and LuxI non-*ssrA* (blue, strain 1) tagged versions of the circuit. See Supplementary Information for complete model information.

Data Fig. 1a, b). Given the ultimate goal of implementation in an *in vivo* microenvironment characterized by variable growth conditions, we tested a range of incubation temperatures (36 °C to 40 °C) and perfusion rates (100 $\mu\text{m s}^{-1}$ to 200 $\mu\text{m s}^{-1}$), measuring an average period of 3 h across all conditions (Fig. 1d). These findings demonstrate that the SLC has the capacity to generate robust cycles of bacterial lysis in our microfluidic devices across a spectrum of environmental fluctuations that is likely to exist in an *in vivo* context.

The emergence of bacterial therapies in synthetic biology has accentuated the need for predictive modelling. This need stems from a bottleneck created by a difference in the timescales for bacterial cloning versus animal experiments; the circuits required for candidate therapies can be created much faster than they can be tested *in vivo*. Therefore, in order to quantitatively characterize the SLC concept before testing in animal models, we developed a computational model (Fig. 2a and Supplementary Information) to define an optimal strategy for subsequent testing in a lower-throughput animal model setting. We found that high production and degradation rates of the feedback-controlling proteins resulted in a wider domain of oscillatory dynamics in the parameter space (Fig. 2b). This model is consistent with our observations that oscillations in *S. Typhimurium* were more robust than in *Escherichia coli*, in which rates of protein production and degradation were previously found to be lower¹⁶ (Extended Data Fig. 1c and Supplementary Video 3). As the ability to manipulate circuit behaviour enhances the versatility of the system, we explored the tunability of the lysis period by adding an *ssrA* degradation tagging sequence on the LuxI protein. Consistent with model predictions, we observed an increased period and colony firing amplitude when tracking bacterial population dynamics (Fig. 2c, d and Extended Data Fig. 1d). The SLC thus enables tuning of the period and magnitude of delivery, which will be necessary for eventual application of this platform in the complex and fluctuating conditions present *in vivo*.

To incorporate a cytotoxic payload into the SLC strain, we added expression of Haemolysin E, encoded by *hlyE* of *E. coli*, which has been tested as a pore-forming anti-tumour toxin¹⁷. We initially confirmed the capability of the circuit to release intracellular contents by visualizing released sfGFP with a small microfluidic sink located beneath the growth chamber (Extended Data Fig. 2a–c). Then to visualize bacterial lysis and killing of cancer cells *in vitro* via HlyE, we engineered a microfluidic device so that cancer cells adhere inside a growth channel that is flanked by smaller bacterial growth chambers, which permits simultaneous single-cell visualization of bacterial lysis and cancer cell death (Extended Data Fig. 2d). After co-culturing human cervical

cancer HeLa cells with *S. Typhimurium* harbouring the SLC circuit, we observed HeLa cell death upon the onset of bacterial lysis, indicating efficient toxin release (Fig. 3a, b and Supplementary Videos 4 and 5). Complete cell death occurred in the growth channel within ~ 111 min of initial sfGFP fluorescence (Fig. 3c). Thus, the SLC bacteria were capable of releasing HlyE at levels necessary to kill tumour-derived cells.

We assessed the toxicity of released SLC or control bacterial contents in batch culture. As anticipated, we found that HeLa cells exposed to supernatant from a culture of the SLC bacteria bearing the *hlyE* module exhibited almost complete loss of viability (Fig. 3d), whereas the viability of HeLa cells exposed to supernatants of bacteria bearing the *hlyE* module without the SLC and equivalent dose of non-payload bearing SLC bacteria were only slightly affected ($\sim 15\%$). We concluded that bacterial lysis allowed for efficient HlyE release *in vitro* and that natural intracellular bacterial contents do not significantly affect HeLa cell viability. We further investigated the delivery characteristics of the SLC bacteria with *hlyE* by seeding variable amounts of circuit-harboring bacteria with HeLa cultures in well plates. We observed that the time to HeLa cell death following initial seeding increased with lower bacterial seeding volumes, presumably resulting from the extended time needed for bacteria to reach the quorum threshold (Fig. 3e and Supplementary Video 6). Initial seeding with a larger volume of bacteria resulted in increased firing rates which corresponded to shorter HlyE exposure times until cell death, consistent with a greater magnitude of lysis and payload release, although the cumulative toxicity threshold appears to be similar in all cases (Fig. 3f). On the basis of these observations, the seeding size of the bacterial population can be adjusted to determine the initial timing and release characteristics of the circuit.

We used a luciferase reporter to monitor bacterial population dynamics in grafted syngeneic colorectal tumours in mice. To minimize the extent of plasmid loss in the absence of antibiotic selection *in vivo*, we incorporated previously described stabilizing elements for plasmid retention and segregation into the SLC strain^{18–22}. Additionally, we placed both the payload and *luxCDABE* genes (the *in vivo* reporter module) under the *luxI* promoter as an indicator of *hlyE* production and quorum firing via bacterial luminescence (Fig. 1a). Using a subcutaneous model of colorectal cancer (MC26 cell line) in immunocompetent mice, we intratumorally injected a strain of SLC bacteria (SLC-*hly*). We observed pulsatile bacterial population dynamics within the tumour (Fig. 4a–c and Extended Data Fig. 3a, b) using *in vivo* imaging technology²³, consistent with the design and *in vitro* characterization (Fig. 2). The end luminescence intensity was on

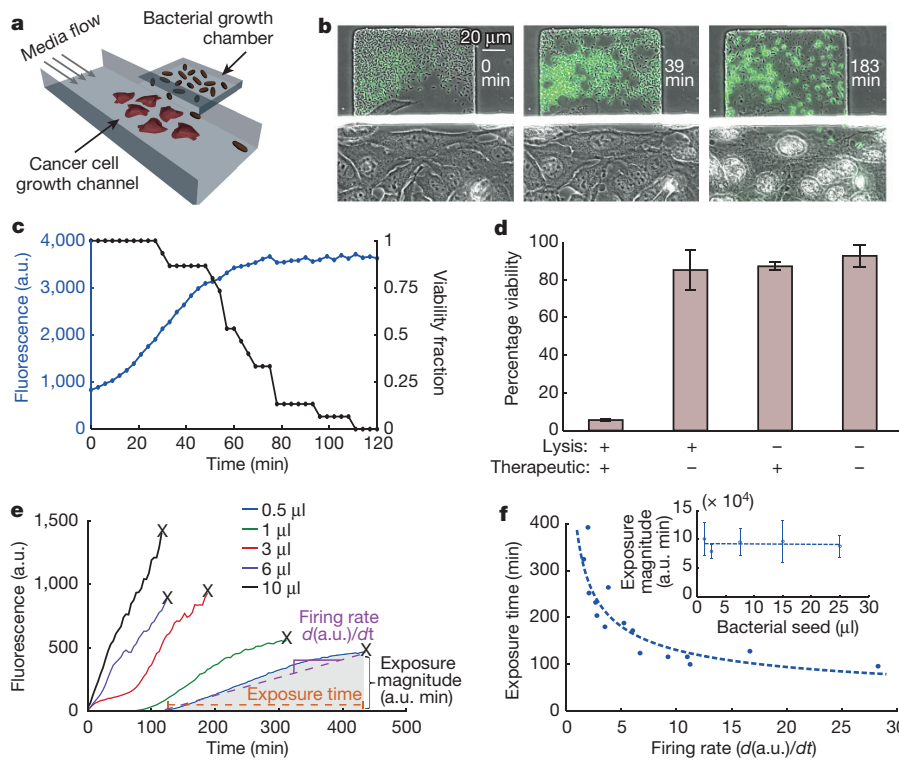


Figure 3 | *In vitro* co-culture. **a**, Schematic of the microfluidic co-culture with cancer cells and bacteria. Fluidic resistance was modified in this chip to achieve stable near-stagnant flow reduction to allow for cancer cell adherence and for diffusion of released therapeutic from the trap to the channel (see Supplementary Information). **b**, Frames from the co-culture time series sequentially visualizing *S. Typhimurium* (strain 3) firing, lysis and HeLa cell death. **c**, Fluorescent profile of the bacteria and HeLa cell viability fraction (number of live cells / number of dead cells in image frames) from **b** with time. **d**, Percentage viability of HeLa cells co-cultured with supernatant from *S. Typhimurium* culture harbouring the SLC + HlyE (strain 4), the SLC only (strain 5), constitutive *hlyE* only (strain 6), or no plasmid (strain 7). Error bars indicate ± 1 s.e. averaged over three measurements. **e**, Fluorescence profile of the SLC + HlyE (strain 4) co-cultured with HeLa cells at various initial seeding densities. The x symbols on the graph mark the point of complete HeLa cell death. **f**, The toxin exposure time, measured from the initial presence of fluorescence to HeLa cell death, as a function of the sfGFP production rate (see example in **e**). Although the time to death depends on seeding, the total magnitude of exposure remains conserved (inset). Error bars indicate ± 1 s.e. for three measurements. See Supplementary Information for ELH1301 host strain information.

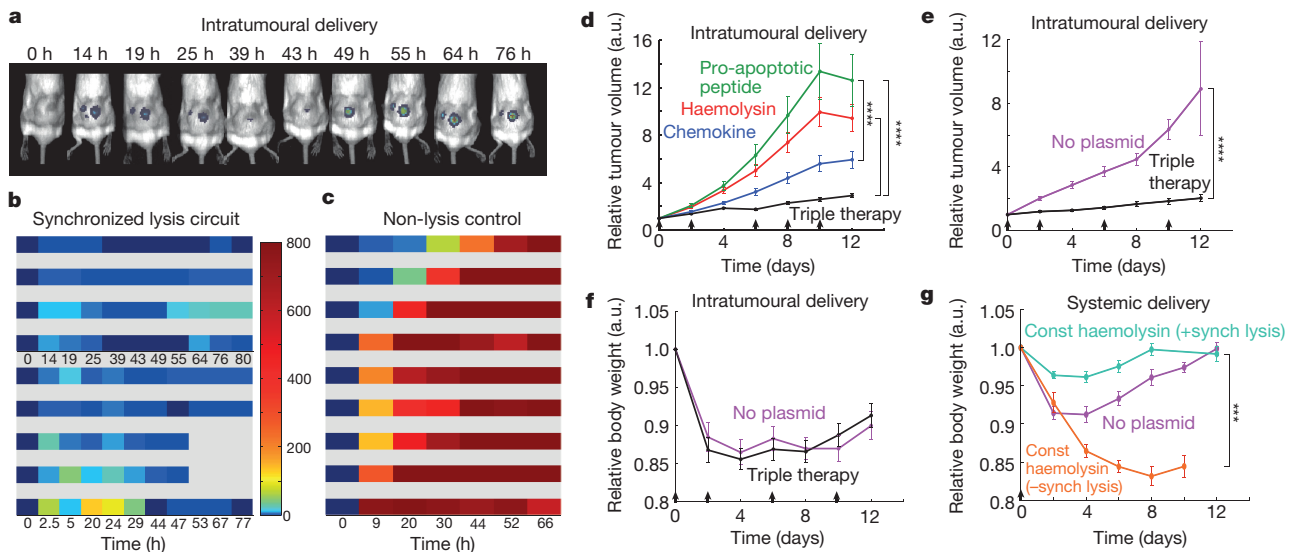


Figure 4 | *In vivo* bacterial dynamics, effect on tumours and tolerability in a subcutaneous tumour model. **a**, *In vivo* imaging over time of a mouse bearing two hind flank tumours injected once with the stabilized SLC-hly strain (strain 8). **b**, Single tumour density map trajectories of bacterial luminescence (relative to luminescence at 0 h) for the SLC-hly strain (strain 8). Data for each axis represents separate experiments. **c**, Single tumour density map trajectories of bacterial luminescence for the genomically integrated constitutively luminescent strain (strain 9). Intratumoural injection resulted in over 35-fold higher post-injection luminescence compared to intravenous injection (Extended Data Fig. 3d). **d**, Average relative tumour volume over time for subcutaneous tumour bearing mice injected with SLC-hly (red, strain 10), SLC-cdd (green, strain 14), SLC-ccl21 (blue, strain 15), and all together (SLC-3) (black). Bacteria were injected intratumourally on days 0, 2, 6, 8, and 10 (black arrows) ($***P < 0.0001$, two-way ANOVA with Bonferroni post-test, $n = 14-17$ tumours, error bars show s.e.). **e**, Average relative tumour volume over

time for mice with subcutaneous tumours injected with the SLC-3 strains (black, strains 10, 14 and 15) and the no-plasmid control (magenta, strain 7). Bacteria were injected intratumourally on days 0, 2, 6, and 10 (black arrows) ($***P < 0.0001$, two-way ANOVA with Bonferroni post-test, $n = 18-19$ tumours, error bars represent s.e.). **f**, Average relative body weight over time for mice with subcutaneous tumours injected with the SLC-3 strains (black, strain 10, 14, and 15) and the no-plasmid control (magenta, strain 7). Bacteria were injected intratumourally on days 0, 2, 6, and 10 (black arrows) ($n = 10$ mice for both cases, error bars represent s.e.). **g**, Average relative body weight over time for subcutaneous tumour-bearing mice with a single intravenous injection of the SLC + constitutive hlyE (turquoise, $n = 9$ mice, strain 11), a non-SLC strain with constitutive hlyE (orange, $n = 5$ mice, strain 12), or the no-plasmid control strain (magenta, $n = 9$ mice, strain 7) ($***P < 0.001$, two-way ANOVA with Bonferroni post-test, error bars represent s.e.).

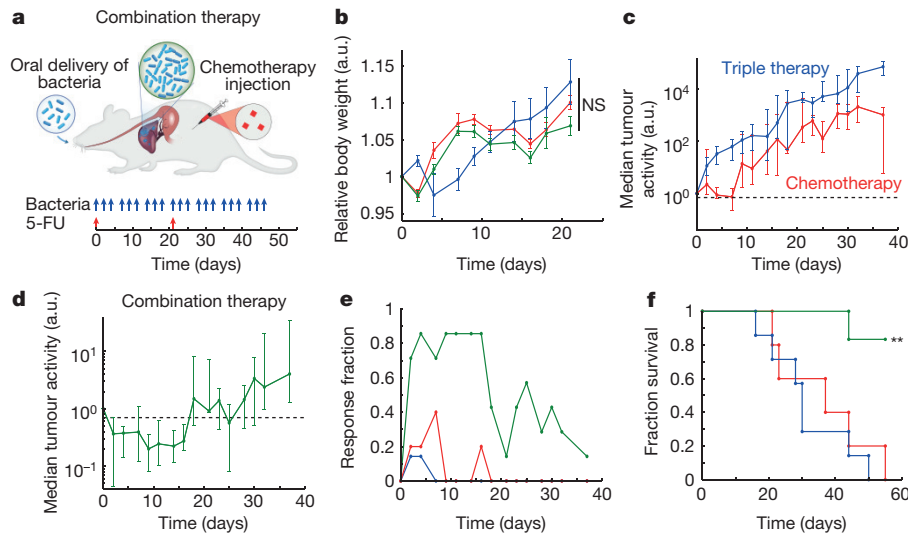


Figure 5 | *In vivo* testing in an experimental model of colorectal metastases in the liver via oral delivery of bacteria. **a**, Schematic of the experimental syngeneic transplantation model of hepatic colorectal metastases in a mouse, with the dosing schedule of either engineered bacteria (SLC-3) or a common cytotoxic chemotherapeutic, the antimetabolite 5-FU. The SLC-3 strains were delivered orally. 5-FU was delivered via intraperitoneal injection. **b**, Relative body weight over time for the mice with hepatic colorectal metastases fed with the SLC-3 strains (blue), injected with 5-FU chemotherapy (red), or a combination of the

two (green). Error bars indicate ± 1 s.e. for 5–7 mice. **c**, Median relative tumour activity, measured via tumour cell luminescence using *in vivo* imaging, for the chemotherapy and SLC-3 cases from **b**. **d**, Median relative tumour activity for the combination therapy case from **b**. Error bars for **c** and **d** indicate the interquartile ranges for 5–7 mice. The dashed line marks relative tumour activity of 0.70. **e**, Fraction of mice from the cases in **b** which respond with 30% reduction of tumour activity over time. **f**, Fraction survival over time for the mice in **b** (** $P < 0.01$, log rank test; $n = 5–7$ mice).

average ~ 300 -fold lower than the constitutive control strain, indicating a significant decrease in bacterial population levels within the tumour (Extended Data Fig. 3c).

Given the ability to engineer bacterial population dynamics in tumour grafts, we leveraged the versatility of the SLC bacteria as a delivery system to compare different classes of previously developed payloads. In addition to the haemolysin strain that was characterized in microfluidic devices, we created two additional SLC strains expressing genes to activate a host immune response (via T-cell and dendritic cell recruitment, using mouse CCL21) or trigger tumour cell apoptosis (using the cell death domain of Bit1 fused to the tumour-penetrating peptide iRGD, or CDD-iRGD)^{24,25}. Upon intratumoral injection, the immune recruitment strain elicited the strongest effect on tumour growth when compared to the haemolysin or apoptotic strains (Fig. 4d). We observed that an equal mixture of the three strains generated a stronger response than any single strain (Fig. 4d and Extended Data Fig. 3e–g), and on this basis we elected to pursue the ‘triple-strain’ dose for further testing in order to minimize animal usage. In a side-by-side comparison, we observed that the tumour response to SLC triple-strain (SLC-3) injections was significantly larger than the response to unmodified bacteria (Fig. 4e). Upon necropsy, histopathological analysis of remnant tumours was performed for mice treated with the SLC-3 strains, chemotherapy or unmodified bacteria. In mice treated with SLC-3 and non-circuit bacterial strains, robust staining of bacteria was observed by anti-*Salmonella* antibodies, showing localization of *Salmonella* within tumours. TUNEL staining indicated higher levels of apoptosis and cell death in SLC-3 treated tumours (Extended Data Fig. 4).

As a first step towards monitoring the effect of bacterial injections on the host, we compared how the triple-strain system affected body weight when administered intratumorally and intravenously, as the administration route affects bacterial localization (Extended Data Fig. 3d). We found that treatment with the SLC strains generated the same weight change as unmodified bacteria when administered intratumorally (Fig. 4f). However, intravenous administration of the SLC conferred a greater health benefit on the basis of observations that SLC strains producing constitutive therapy were better tolerated

than unmodified bacteria or non-SLC strains producing constitutive therapy (Fig. 4g). Although further targeted studies are required to systematically explore the effect of these bacteria on host health, these preliminary experiments suggest that the SLC design can reduce the burden of bacterial injections.

To explore a proof-of-principle for the application of our circuit in the context of *in vivo* tumours, we examined the efficacy of our system in an experimental syngeneic transplantation model of colorectal metastases within the liver. We had previously established that oral delivery of these bacterial strains led to safe and efficient colonization of hepatic colorectal metastases (see Methods), and that mice tolerated repeated dosing without overt adverse effects (Fig. 5a, b)²². In the context of bacteria-based therapeutic candidates, previous studies have shown that anaerobic bacteria can occupy avascular tumour compartments where chemotherapy is thought to be ineffective due to poor drug delivery¹¹. Thus a synergistic effect may arise when bacteria are used to deliver drugs to the necrotic core of a tumour, while standard chemotherapy is used for the vascularized regions^{11,26}. Inspired by this paradigm, we tested the combination of SLC-3 bacteria with a common clinical chemotherapy of 5-fluorouracil (5-FU). Tumours exhibited similar growth trajectories in response to repeated oral delivery of either the bacterial therapy alone, or two i.v. doses of 5-FU on day 0 and day 21 (Fig. 5c). In contrast, combination of these two applications led to a marked decrease in tumour activity over a period of 18 days, followed by a return to growth (Fig. 5d). During the initial 18-day period, a large fraction of the tumours was scored as eliciting at least a 30% reduction in tumour activity (Fig. 5e). The overall response led to roughly a 50% increase in the mean survival time for animals harbouring incurable colorectal metastases (Fig. 5f). Improvements may arise from strategies for long-term circuit stability or the utilization of additional therapeutic cargo.

The synchronized lysis circuit exemplifies a methodology for leveraging the tools of synthetic biology to exploit the ability of certain bacteria to colonize disease sites. In contrast to most drug delivery strategies, the synchronized lysis paradigm does not require pre-loading of a drug or the engineering of additional secretion machinery. In addition, it has the potential to decrease the likelihood of a systemic

inflammatory response through population control; as the bacterial colony is pruned after each oscillatory lysis event, the design could mitigate an undesirable host response. The circuit may enable new bacterial drug delivery strategies through modulation of the frequency and amplitude of the population cycles over time. Given recent insights into how host metabolism and circadian function are affected by the population dynamics of the gut microbiota, cyclical population control may be a prospective strategy to prevent host disturbances resulting from aberrant oscillations of gut microbes^{27,28}. Such engineering strategies may allow for the development of therapeutic communities within *in vivo* environments in which population dynamics are driven by interacting viruses, bacteria and host immune cells²⁹.

Online Content Methods, along with any additional Extended Data display items and Source Data, are available in the online version of the paper; references unique to these sections appear only in the online paper.

Received 24 January; accepted 13 June 2016.

Published online 20 July 2016.

1. Cho, I. & Blaser, M. J. The human microbiome: at the interface of health and disease. *Nature Rev. Genet.* **13**, 260–270 (2012).
2. Xuan, C. *et al.* Microbial dysbiosis is associated with human breast cancer. *PLoS One* **9**, e83744 (2014).
3. Fischbach, M. A., Bluestone, J. A. & Lim, W. A. Cell-based therapeutics: the next pillar of medicine. *Sci. Transl. Med.* **5**, 179ps7 (2013).
4. Pawelek, J. M., Low, K. B. & Bermudes, D. Tumor-targeted *Salmonella* as a novel anticancer vector. *Cancer Res.* **57**, 4537–4544 (1997).
5. Ruder, W. C., Lu, T. & Collins, J. J. Synthetic biology moving into the clinic. *Science* **333**, 1248–1252 (2011).
6. Weber, W. & Fussenegger, M. Emerging biomedical applications of synthetic biology. *Nature Rev. Genet.* **13**, 21–35 (2011).
7. Baban, C. K., Cronin, M., O'Hanlon, D., O'Sullivan, G. C. & Tangney, M. Bacteria as vectors for gene therapy of cancer. *Bioeng. Bugs* **1**, 385–394 (2010).
8. Hopton Cann, S. A., van Netten, J. P. & van Netten, C. Dr William Coley and tumour regression: a place in history or in the future. *Postgrad. Med. J.* **79**, 672–680 (2003).
9. Davila, M. L. *et al.* Efficacy and toxicity management of 19–28z CAR T cell therapy in B cell acute lymphoblastic leukemia. *Sci. Transl. Med.* **6**, 224ra25 (2014).
10. Garrett, W. S. Cancer and the microbiota. *Science* **348**, 80–86 (2015).
11. Dang, L. H., Bettgeowda, C., Huso, D. L., Kinzler, K. W. & Vogelstein, B. Combination bacteriolytic therapy for the treatment of experimental tumors. *Proc. Natl Acad. Sci. USA* **98**, 15155–15160 (2001).
12. Danino, T., Mondragón-Palomino, O., Tsimring, L. & Hasty, J. A synchronized quorum of genetic clocks. *Nature* **463**, 326–330 (2010).
13. Prindle, A. *et al.* A sensing array of radically coupled genetic 'biopixels'. *Nature* **481**, 39–44 (2011).
14. Young, K. D. & Young, R. Lytic action of cloned φ X174 gene E. *J. Virol.* **44**, 993–1002 (1982).
15. Marguet, P., Tanouchi, Y., Spitz, E., Smith, C. & You, L. Oscillations by minimal bacterial suicide circuits reveal hidden facets of host-circuit physiology. *PLoS One* **5**, e11909 (2010).
16. Prindle, A. *et al.* Genetic circuits in *Salmonella typhimurium*. *ACS Synth. Biol.* **1**, 458–464 (2012).
17. Ryan, R. M. *et al.* Bacterial delivery of a novel cytotoxin to hypoxic areas of solid tumors. *Gene Ther.* **16**, 329–339 (2009).
18. Gerdes, K. The *parB* (*hok/sok*) locus of plasmid R1: a general purpose plasmid stabilization system. *Nature Biotechnol.* **6**, 1402–1405 (1988).
19. Wood, T., Kuhn, R. & Peretti, S. Enhanced plasmid stability through post-segregational killing of plasmid-free cells. *Biotechnol. Tech.* **4**, 39–44 (1990).
20. Derman, A. I. *et al.* Phylogenetic analysis identifies many uncharacterized actin-like proteins (Alps) in bacteria: regulated polymerization, dynamic instability and treadmilling in Alp7A. *Mol. Microbiol.* **73**, 534–552 (2009).
21. Danino, T., Lo, J., Prindle, A., Hasty, J. & Bhatia, S. N. *In vivo* gene expression dynamics of tumor-targeted bacteria. *ACS Synth. Biol.* **1**, 465–470 (2012).
22. Danino, T. *et al.* Programmable probiotics for detection of cancer in urine. *Science Transl. Med.* **7**, 289ra84 (2015).
23. Danino, T., Prindle, A., Hasty, J. & Bhatia, S. Measuring growth and gene expression dynamics of tumor-targeted *S. Typhimurium* bacteria. *JoVE* e50540 (2013).
24. Chen, R. *et al.* Application of a proapoptotic peptide to intratumorally spreading cancer therapy. *Cancer Res.* **73**, 1352–1361 (2013).
25. Loeffler, M., Le'Negrate, G., Krajewska, M. & Reed, J. C. *Salmonella typhimurium* engineered to produce CCL21 inhibit tumor growth. *Cancer Immunol. Immunother.* **58**, 769–775 (2009).
26. Forbes, N. S. Engineering the perfect (bacterial) cancer therapy. *Nature Rev. Cancer* **10**, 785–794 (2010).
27. Leone, V. *et al.* Effects of diurnal variation of gut microbes and high-fat feeding on host circadian clock function and metabolism. *Cell Host Microbe* **17**, 681–689 (2015).
28. Thaiss, C. A., Levy, M. & Elinav, E. Chronobiomics: the biological clock as a new principle in host–microbial interactions. *PLoS Pathog.* **11**, e1005113 (2015).
29. Cheong, I. *et al.* A bacterial protein enhances the release and efficacy of liposomal cancer drugs. *Science* **314**, 1308–1311 (2006).

Supplementary Information is available in the online version of the paper.

Acknowledgements The UCSD team was supported by the National Institute of General Medical Sciences of the National Institutes of Health (R01GM069811) and the San Diego Center for Systems Biology (P50 GM085764). The MIT team was supported by a Koch Institute Support Grant (P30-CA14051) from the National Cancer Institute (Swanson Biotechnology Center), a Core Center Grant (P30-ES002109) from the National Institute of Environmental Health Sciences, the Ludwig Center for Molecular Oncology at MIT and an Amar G. Bose Research Grant. T.D. was supported by the Mirrock Postdoctoral fellowship and the NIH Pathway to Independence Award NIH (K99 CA197649-01). A.P. was supported by the Department of Defense National Defense Science and Engineering Graduate Fellowship and holds a Simons Foundation Fellowship of the Helen Hay Whitney Foundation and a Career Award at the Scientific Interface from the Burroughs Wellcome Fund. S.N.B. is an HHMI Investigator. We would like to thank R. Johnson for help with constructing microfluidic devices, H. Fleming for help with editing the manuscript, and H. Ding of The Barbara K. Ostrom (1978) Bioinformatics and Computing Facility in the Swanson Biotechnology Center for help with the statistical tests carried out in this study. We would also like to thank L. You for providing the lysis gene used in this study.

Author Contributions M.O.D. and J.H. designed the synchronized lysis circuit. M.O.D., J.S., L.S.T. and J.H. developed the computational model. M.O.D. and A.P. built and tested the bacterial circuit in microfluidics and performed the co-culture experiments. M.O.D. and E.J. collected the viability data, and M.O.D. and J.H. analysed the bacterial circuit data. T.D., M.S., K.A., and E.A. designed and performed the *in vivo* experiments. M.O.D., T.D., A.P., S.N.B., and J.H. analysed the animal data, and wrote and edited the manuscript.

Author Information Reprints and permissions information is available at www.nature.com/reprints. The authors declare no competing financial interests. Readers are welcome to comment on the online version of the paper. Correspondence and requests for materials should be addressed to J.H. (jhasty@eng.ucsd.edu).

Reviewer Information *Nature* thanks R. Solé, B. Vogelstein and the other anonymous reviewer(s) for their contribution to the peer review of this work.

METHODS

Strains and plasmids. Our circuit strains were cultured in LB media with $50 \mu\text{g ml}^{-1}$ and $34 \mu\text{g ml}^{-1}$ of kanamycin and chloramphenicol respectively, along with 0.2% glucose, in a 37°C incubator. Mammalian cells (HeLa CCL-2 from ATCC, verified by third-party cell line authentication services using an STR multiplex system) were cultured in DMEM media supplemented with 10% fetal bovine serum and 1% penicillin/streptomycin (CellGro 30-002-CI), placed inside a tissue culture incubator at 37°C maintained at 5% CO_2 . Plasmids were constructed using the CPEC method of cloning or using standard restriction digest/ligation cloning. The activator plasmid (Kan, ColE1) was used in previous work from our group, and the lysis plasmid was constructed by taking the lysis gene, *E*, from the ePop plasmid via PCR and cloning it into a vector (Chlor, p15A) under the control of the *luxI* promoter^{13,15}. The *hlyE* gene was obtained via PCR from the genomic DNA of MG1655, while mouse CCL21 and CDD-iRGD were synthesized. These genes were cloned into the lysis plasmid, under the control of either the *tac* or *luxI* promoters (Extended Data Fig. 5). Co-culturing was performed with HeLa cells and either motile or non-motile *S. Typhimurium*, SL1344 (Extended Data Table 1). For full strain and plasmid information, please refer to the Supplementary Information.

Microfluidics and microscopy. The microfluidic devices and experiment preparation protocols used in this study are similar to those previously reported from our group¹³. The bacteria growth chambers were $100 \times 100 \mu\text{m}$ in area and approximately $1.4 \mu\text{m}$ in height. For co-culture experiments on the chip, we first loaded a suspended culture of HeLa cells in the device media channels at very low flow rates, to allow for adherence, and then incubated the device in a tissue culture incubator for 0.5–2 days to allow for proliferation. On the day of the experiment, the device was transferred to the microscope and circuit-containing bacteria were loaded in the growth chambers before imaging. Acquisition of images was performed with a Nikon TI2 using a Photometrics CoolSnap cooled CCD camera. The scope and accessories were programmed using the Nikon Elements software.

Co-cultures for well plate experiments were performed in Falcon 96-well tissue culture plates. HeLa cells were allowed to adhere to the wells before the addition of bacteria and subsequent imaging under the microscope or measurement in a TECAN Infinite M200 Pro plate reader. For viability measurements using an MTT assay, there were two technical replicates per well. For fluorescence measurements of co-cultures with variable seeding densities of bacteria, there were three technical replicates per case.

Additional details on microfluidics and microscopy can be found in the Supplementary Information.

In vivo experiments. All animal work was approved by the committee on animal care (MIT, protocol 0414-022-17). The protocol requires animals to be euthanized when tumors reach 2 cm^3 , or under veterinary staff recommendation. The cell line (MC26-LucF, Tanabe laboratory, Massachusetts General Hospital) was obtained from, and authenticated by, the Tanabe laboratory, MGH. The cell line was tested several times to be mycoplasma-free before implantation in mice. Sample sizes for mice were determined by expected effect size to produce a power of 0.8–0.9. Mice were blindly randomized into various groups using a random number generator.

Subcutaneous tumour model. Animal experiments were performed on 6-week-old female BALB/c mice (Taconic Biosciences) with bilateral subcutaneous hind flank tumours from an implanted mouse colon cancer cell line. The concentration for implantation of the tumour cells was 10^8 cells per ml in DMEM (no phenol red). Cells were then implanted subcutaneously at a volume of $100 \mu\text{l}$ per flank, with each implant consisting of 10^7 cells. Tumours were typically grown to an average of 300 mm^3 before experiments.

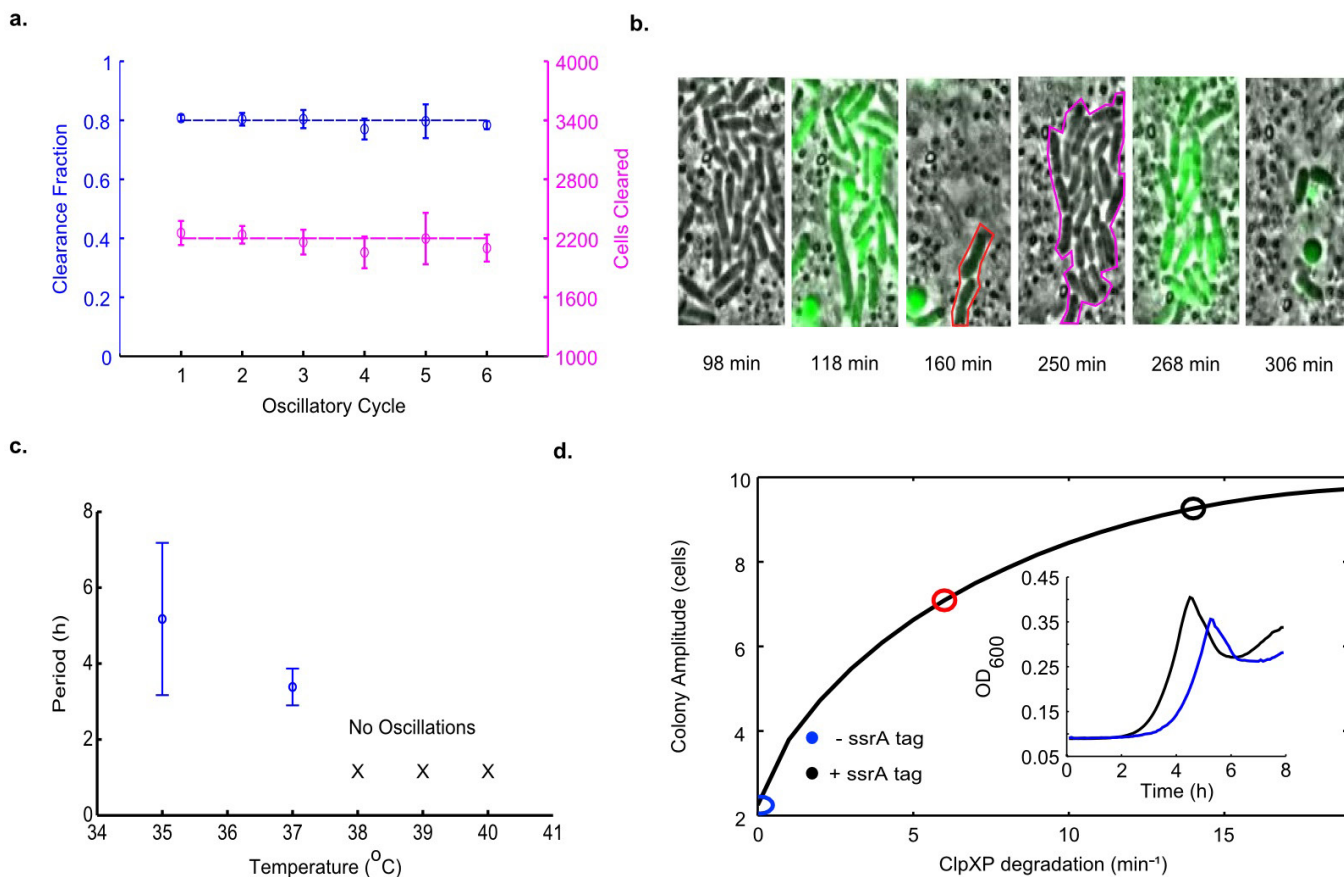
Experimental liver metastasis model. The experimental metastasis model was generated by injecting luciferase-producing mouse cancer cells into surgically externalized spleens of immunocompetent mice. Tumour cells seeded the liver during 90 s, after which the spleen was removed to prevent ectopic tumour growth³⁰. The MC26-LucF cell line was used (Tanabe Laboratory, MGH) and injected at 5×10^4 cells per $100 \mu\text{l}$ PBS into the spleens of female BALB/c mice at 6 weeks of age (Taconic Biosciences.). For the liver metastasis model, tumours were grown for 5–7 days to an average total tumour burden of 143 mm^3 before experiments.

Bacterial growth and administration. Bacterial strains were grown overnight in LB media containing appropriate antibiotics and 0.2% glucose as for the *in vitro* experiments. A 1:100× dilution in fresh media with antibiotics was started the day of injection and grown until an OD < 0.1 to prevent bacteria from reaching the quorum threshold (for SLC specifically). Bacteria were spun down and washed 2 to 3 times with sterile PBS before injection into mice. Intratumoural injections of bacteria were performed at a concentration of 5×10^7 cells per ml in PBS with a total volume of 10–20 μl injected per tumour, while intravenous injections were given at a total volume of $100 \mu\text{l}$. For the SLC-3 strains injection, this final volume was equally divided between the three strains at the indicated density. For liver metastasis experiments, bacteria were grown in LB media containing appropriate antibiotics and 0.2% glucose until they reached an OD of 0.05, after which they were concentrated to 10^9 to 5×10^9 bacteria per ml and delivered via oral gavage.

Post-administration monitoring for subcutaneous liver metastasis models. Luminescent signal was measured with the IVIS spectrum *in vivo* imaging system following bacterial injection. Measurements were compared relative to pre-injection values to follow dynamics. Subcutaneous tumour volume was quantified using calipers to measure the length, width, and height of each tumour throughout the imaging course ($V = L \times W \times H$). Volumes were compared to pre-injection values to follow physical tumour growth. Survival of mice was measured as the time from the beginning of the experiment up to the day when mice were moribund and euthanized. Survival for the experiment in Fig. 4f was measured with two biological replicates.

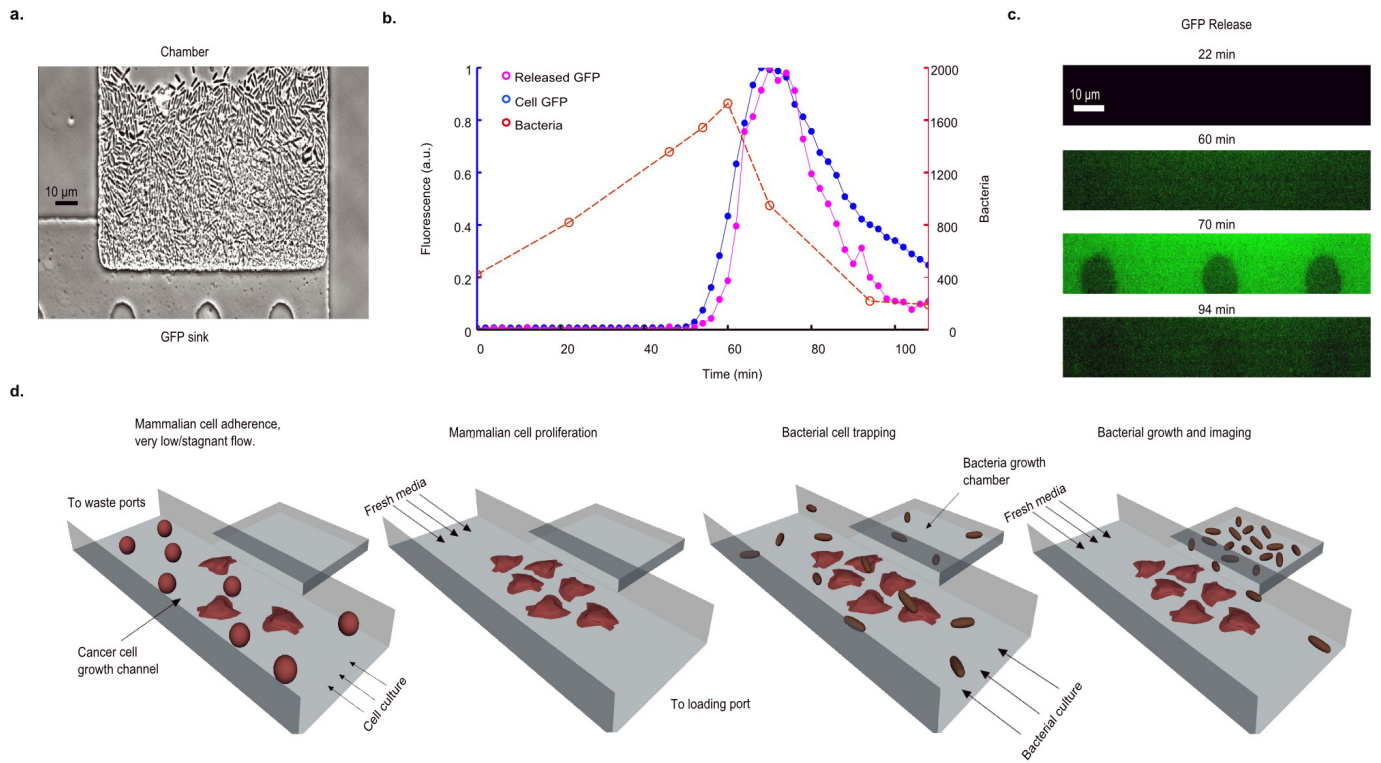
Statistical analysis. Statistical tests were calculated either in Excel (Student's *t*-test) or GraphPad Prism 5.0 (ANOVA with Bonferroni post-test, log-rank test). The details of the statistical tests carried out are indicated in the respective figure legends. Where data were approximately normally distributed, values were compared using either a Student's *t*-test or one-way ANOVA for single variable, or a two-way ANOVA for two variables. Mice were randomized in different groups before experiments.

30. Soares, K. C. *et al.* A preclinical murine model of hepatic metastases. *JoVE* e51677 (2014).



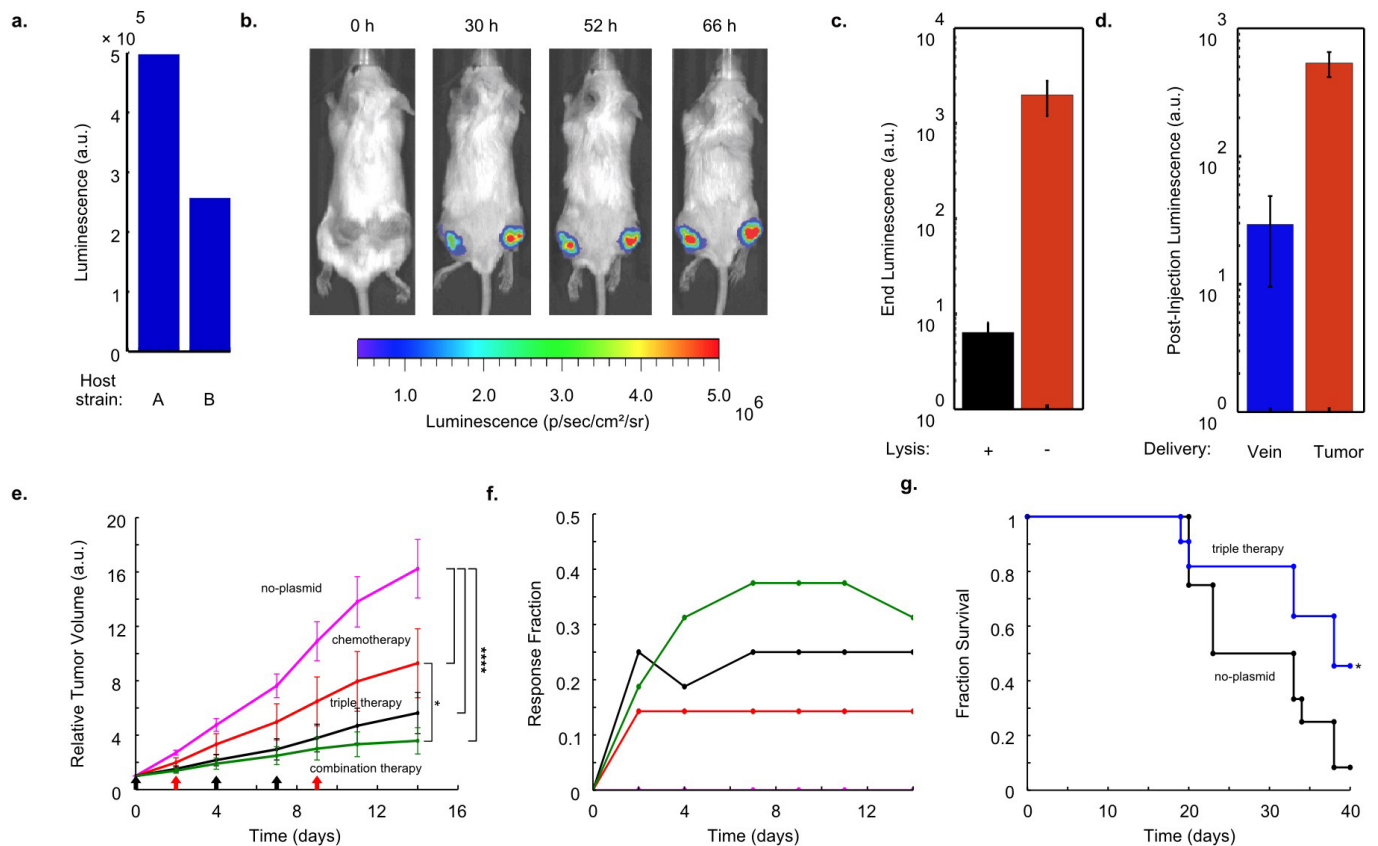
Extended Data Figure 1 | Various properties of the SLC. **a**, The fraction and number of bacterial cells cleared per consecutive oscillatory cycle in the growth chamber for a typical microfluidic experiment for *S. typhimurium*, including the effects of lysis and flow of cells outside of the trap (strain 1). **b**, Subset of time series images from the experiment in **a** showing a portion of the growth chamber where survivors of the initial lysis event (160 min frame, red outline) produce progeny (250 min frame, magenta outline) which are lysis sensitive. **c**, Period as a function of the

environmental temperature for *E. coli* (strain 13). The circuit does not oscillate for temperatures above 37 $^{\circ}\text{C}$ in *E. coli*. Error bars indicate ± 1 s.d. for 12–19 peaks. **d**, Colony amplitude at quorum firing for increasing degradation on the LuxI activator protein in the computational model. These simulation results are supported by batch well-plate experiments of the LuxI ssrA (black, strain 2) and non-ssrA (blue, strain 1) tagged versions of the circuit in *S. Typhimurium* (inset).



Extended Data Figure 2 | Investigating lysis-mediated intracellular release. **a**, A bacterial growth chamber with a $0.4\ \mu\text{m}$ high sink for sfGFP visualization after release. **b**, Number of bacteria (red), bacterial fluorescence (blue), sink fluorescence (pink) for a typical oscillatory

cycle (strain 1). **c**, Fluorescence time series images of the microfluidic sink from **b**. **d**, General procedure for performing bacterial and cancer cell co-culture experiments in a microfluidic device (also see Supplementary Information).

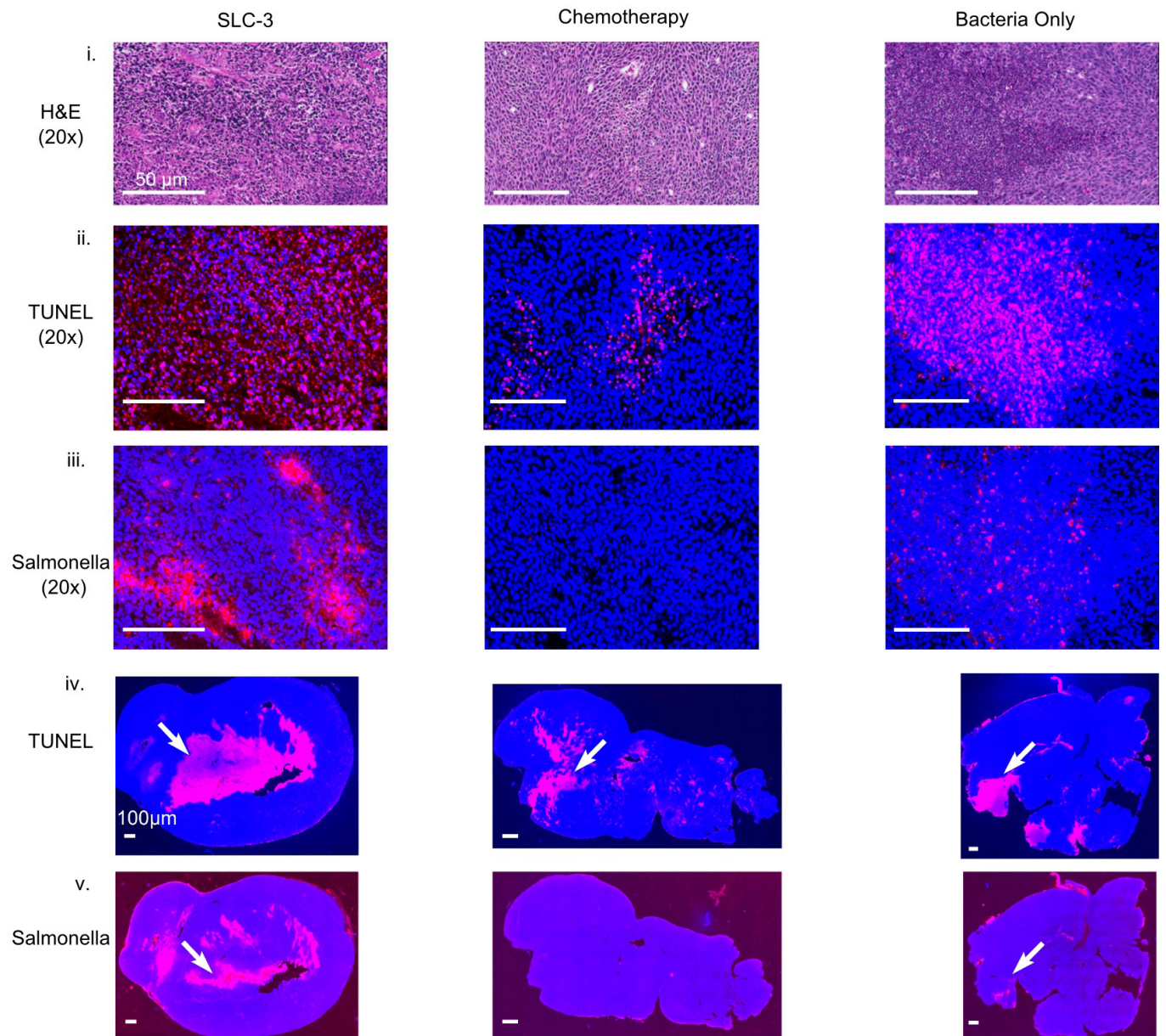


Extended Data Figure 3 | *In vivo* expression and therapy testing.

a. End-point *in vitro* luminescence intensity for SLC strains after ~20 h of growth. Host strains A and B are the host bacteria for strains 8 and 10. They are ELH1301 and ELH 430, respectively. Host A exhibits around twofold higher luminescence with the same circuit than host B. **b.** *In vivo* imaging over time of a mouse bearing subcutaneous tumours injected with a genomically integrated constitutively luminescent strain (strain 9). **c.** End-point *in vivo* bacterial luminescence of the SLC-hly strain and the constitutively luminescent strain from the experiments presented in Fig. 4. Error bars represent the s.e.m. bacterial luminescence from 9 tumours. **d.** Post-injection *in vivo* bacterial luminescence for the constitutively luminescent strain administered intravenously (vein) or intratumorally (tumour). Luminescence was measured ~20 h post-injection. Error bars

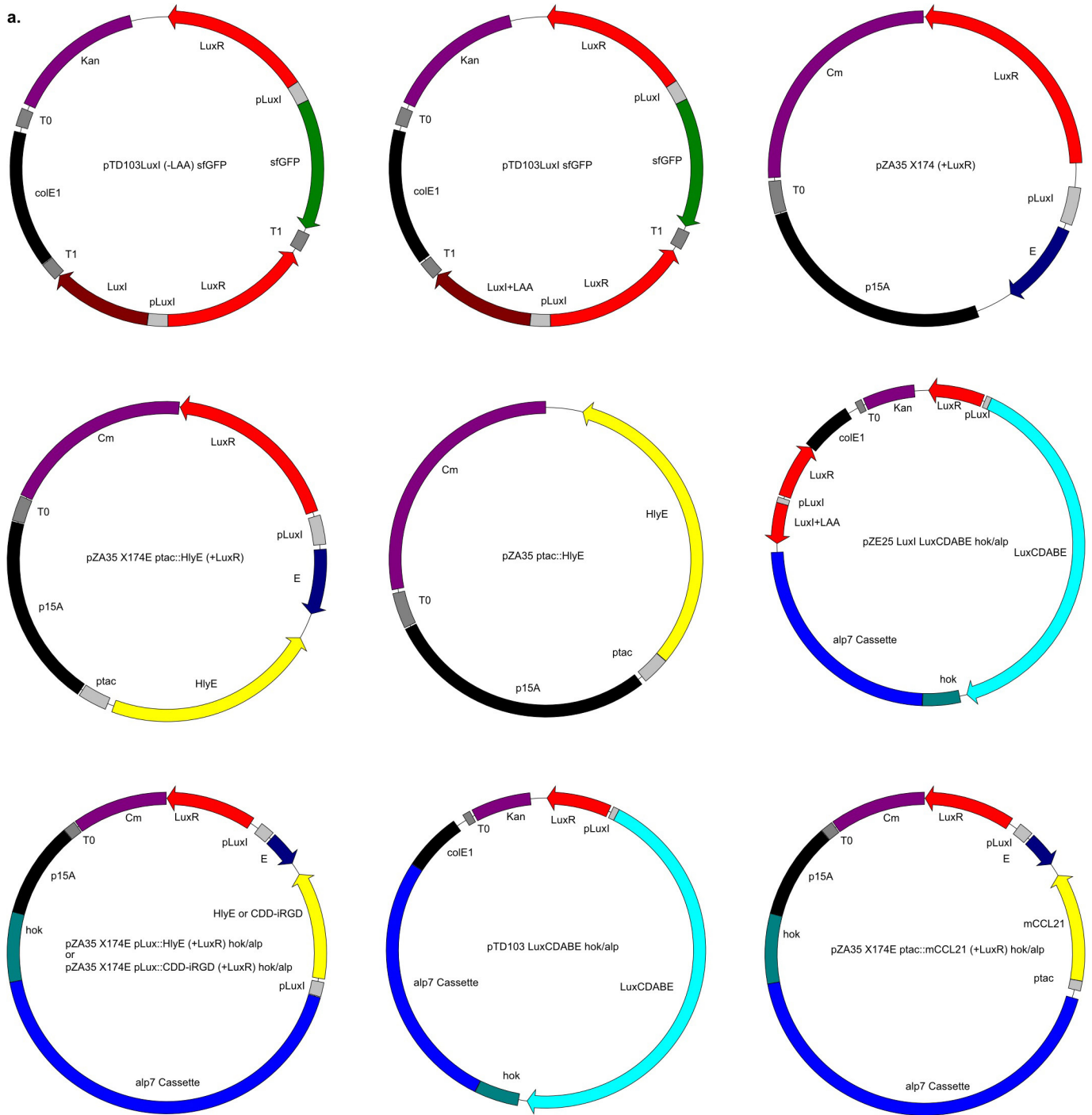
represent s.e.m. bacterial luminescence from 6 and 9 tumours for the intravenous and intratumoural cases, respectively. **e.** Average relative tumour volume over time for subcutaneous tumour bearing mice injected with the no-plasmid bacterium (strain 7), 5-FU chemotherapy, the SLC-3 strains, and the combination of SLC-3 with chemotherapy. Bacteria were injected intratumorally on days 0, 4, and 7 (black arrows), and chemotherapy was administered on days 2 and 9 (red arrows) (* $P < 0.05$, **** $P < 0.0001$, two-way ANOVA with Bonferroni post-test, $n = 12-16$ tumours, error bars represent s.e.). **f.** Fraction of mice from the cases in **e** which respond with 30% reduction of tumour volume over time. **g.** Fraction survival over time for mice with hepatic colorectal metastases fed with either the SLC-3 strains (blue) or the no-plasmid control (black) (* $P < 0.05$, log rank test; $n = 11-12$ mice).

a.

**Extended Data Figure 4 | Histological analysis of tumour sections.**

a. Histology of tumour sections taken from mice with different treatments 3 days post-administration. Haematoxylin and eosin staining for tissue sections intravenously injected with a combination of therapeutic bacteria (SLC-3), chemotherapy (5-FU), or a bacteria control with no therapeutic (strain 7) (i); TUNEL staining (red) in the same sections indicating cell apoptosis (ii); *Salmonella* immunohistochemistry (red) in the same sections confirming presence of bacteria in tumours (iii). Scale bars for (i–iii) denote 50 µm. TUNEL (iv) and *Salmonella* (v) staining (red) in

the entire tumour sections (examples indicated by arrows). Scale bars for iv and v denote 100 µm. DAPI staining (blue) was used to obtain a measure of live and dead cells in ii–iv. Histology slices ($n = 6$) from 20× images were compared across the groups and mean intensity of TUNEL staining, normalized by sample area, was demonstrated to be significantly higher for SLC-3 compared to the other two groups ($P < 0.0001$, one-way ANOVA), and not significantly different between the chemotherapy and bacteria-only cases.



Extended Data Figure 5 | The main plasmids used in this study. See Supplementary Information for more details.

Extended Data Table 1 | A list of strains and respective plasmids used in this study

Strain #	Strain Name	Host Bacterium	Plasmid(s)
1	MOD47	SL1344, M913	pTD103 luxI (-LAA) sfGFP + pZA35 X714E (+LuxR)
2	MOD46a	SL1344, M913	pTD103 luxI sfGFP + pZA35 X714E (+LuxR)
3	MOD67	SL1344, M913	pTD103 luxI (-LAA) sfGFP + pZA35 X714E (+LuxR) ptac::HlyE
4	MOD61	SL1344, ELH1301	pTD103 luxI sfGFP + pZA35 X714E (+LuxR) ptac::HlyE
5	MOD64	SL1344, ELH1301	pTD103 luxI sfGFP + pZA35 X714E (+LuxR)
6	MOD65	SL1344, ELH1301	pZA35 ptac::HlyE
7	ELH1301	SL1344, ELH1301	N/A
8	MOD105	SL1344, ELH430	pZE25 luxI luxCDABE hok/alp + pZA35 X714E (+LuxR) pLux::HlyE hok/alp
9	EcN-luxCDABE	Nissle 1917	N/A
10	MOD101	SL1344, ELH1301	pZE25 luxI luxCDABE hok/alp + pZA35 X714E (+LuxR) pLux::HlyE hok/alp
11	MOD102	SL1344, ELH1301	pZE25 luxI luxCDABE hok/alp + pZA35 X714E (+LuxR) ptac::HlyE hok/alp
12	MOD69	SL1344, ELH1301	pTD103 LuxCDABE hok/alp + pZA35 X714E (+LuxR) ptac::HlyE hok/alp
13	MOD29	JS006, BW25113	pTD103 luxI sfGFP + pZA35 X714E (+LuxR)
14	MOD110	SL1344, ELH1301	pZE25 luxI luxCDABE hok/alp + pZA35 X714E (+LuxR) pLux::CDD-iRGD hok/alp
15	MOD112	SL1344, ELH1301	pZE25 luxI luxCDABE hok/alp + pZA35 X714E (+LuxR) ptac::mCCL21 hok/alp

See Supplementary Information for more details.

Host Strains and Culturing

Strains with our lysis circuit were grown in LB media with $50 \mu\text{g ml}^{-1}$ and $34 \mu\text{g ml}^{-1}$ of the respective antibiotics (kanamycin and chloramphenicol) along with 0.2% glucose in a 37°C shaking incubator. The glucose was added in order to decrease expression from the Lux promoters. There is a binding site for the CAP-cAMP activating complex located between the *luxI* and *luxR* promoters, which is believed to activate transcription of the *luxR* promoter¹. When glucose levels in the cell are high, levels of cAMP are low, decreasing the transcriptional activation from CAP-cAMP.

For the microfluidics experiments we selected a non-motile *S. typhimurium* host for our circuit, SL1344 (M913: *fliGHI* mutant)². For well-plate co-culture experiments and *in vivo* experiments, we utilized an attenuated *S. typhimurium* host, SL1344 (ELH1301: $\Delta\text{phoPQ } \Delta\text{aroA}$)³, that was shown in previous work to have good efficiency in plasmid retention⁴. For *in vivo* experiments where the luminescence expression of the circuit was measured, we utilized another attenuated strain of *S. typhimurium* SL1344 as the circuit host (ELH430: ΔphoPQ) where luminescence expression was higher (see Extended Data Fig. 3a). For the constitutive luminescence case we used a well characterized bacterium with a constitutive luminescence cassette, *E. coli* Nissle 1917 integrated with p16Slux⁵. A list of strains and plasmids are shown in Extended Data Table 1.

For co-culture experiments, we used the HeLa cell line in DMEM (complete medium) supplemented with 10% fetal bovine serum and appropriate antibiotics for the circuit. HeLa cells were initially grown with penicillin/streptomycin (CellGro 30-002-CI) in the growth medium and placed inside a tissue culture incubator at 37°C with 5% CO_2 before the experiment. For loading on a mi-

crofluidic chip or well-plate, HeLa cells were initially washed with dPBS and dis-adhered with 0.05% or 0.25% trypsin EDTA. Cells were then pelleted and resuspended in DMEM + FBS and the appropriate antibiotics.

Plasmids

Our circuit is composed of two plasmids, an activator plasmid and a lysis/therapeutic plasmid. The main activator plasmid is pTD103LuxI sfGFP which was used in previous work from our group⁶. This plasmid contains the *ssrA*-LAA degradation tag (amino-acid sequence of AANDENYALAA) on LuxI and sfGFP, a superfolder green fluorescent protein variant⁷. pTD103LuxI (-LAA) was constructed by removing the *ssrA*-LAA tag from LuxI. Most of the construction was done using the CPEC method of cloning⁸.

The lysis plasmids were constructed using the modular pZ plasmid set-up with a p15a origin of replication and a chloramphenicol resistance marker⁹. The lysis gene, E from the bacteriophage ϕ X174, was kindly provided by Lingchong You and was taken from the previously reported ePop plasmid via PCR¹⁰. The E gene was placed under the expression of the LuxR-AHL activatable *luxI* promoter. In order to construct the therapeutic versions of the lysis plasmids, we extracted the *hlyE* gene from the genomic DNA of *E. coli* strain MG1655 via PCR and inserted it into the lysis plasmid. The promoter used to drive expression of HlyE was the *tac* promoter for *in vitro* characterization, and the *luxI* promoter for *in vivo* testing. The CDD-iRGD and mCCL21 genes were synthesized as fragments before inserting into the appropriate plasmids.

For the plasmids used in the circuit strains tested *in vivo*, we inserted two stabilizing elements, the hok/sok system and alp7 partitioning system, into the activator and lysis/therapeutic plasmids. Recent work has shown that addition of the hok/sok toxin-antitoxin system and the alp7AR cassette from the *B. subtilis* plasmid pLS20 enables plasmid retention *in vivo*^{11,12}. See Extended Data Fig. 5 for maps of the the plasmids used in this study.

Microscopy and Microfluidics

The microscopy and microfluidics techniques described here are similar to those reported previously from our group¹³. Briefly, our microfluidic devices were constructed from PDMS (polydimethylsiloxane) which was molded and baked on a silicon wafer with micron-scale features formed by cross-linked photoresist. Individual devices (formed by a set of features transferred from the wafer to the PDMS) were then cut out of the baked PDMS and holes were punctured in the devices to allow for the connection of fluid lines. The devices were then bonded onto coverslips and placed on a microscope stage for cell loading and imaging. Fluid lines were connected to the devices from various syringes supplying media, cells, or acting as waste reservoirs. The flow direction in the device was controlled by changing the relative heights between the relevant syringes resulting in hydrostatic pressure driven flow.

We cultured cells to an optical density (A_{600nm}) of approximately 0.1 (using 1.5 ml cuvettes from Plastibrand) before loading a device. Before loading, devices were ‘wetted’ with the media syringes to remove bubbles in the channels¹⁴. Devices were loaded from the cell port by lowering the designated waste port such that the relative changes in height of the cell loading syringe and waste syringe resulted in flow of cells from the cell port to a waste port. Once cells were loaded

in the traps, the flow direction was reversed allowing media to flow into all ports, thus supplying the trapped cells with a continuous perfusion of nutrients. In these microfluidic experiments we added 0.075% Tween20 to the media and cell suspension fluid to prevent cells from adhering to channels and ports within the device. Experiments for characterizing circuit behavior in Fig. 1-2 were done in a side-trap array device, as described previously¹³. The device used with the GFP sink is also arranged as a side-trap array. See Extended Data Fig. 2a for a schematic of the trap and sink.

For the co-culture experiments on the chip, we utilized the side-trap array device and added fluidic resistance on all of the inlet/outlet ports with sinuous channels to increase the dynamic range of achievable flow rates. For mammalian cell loading, cells were trypsinized, pelleted, and re-suspended in 0.5 - 1.0 mL DMEM+FBS+antibiotics (Kanamycin and Chloramphenicol) before loading. Cells were loaded under a light microscope such that un-adhered cells were localized in the media channels under near-stagnant flow conditions. The microfluidic chip and syringe apparatus was then carefully placed in the CO₂ incubator while avoiding any changes in the relative heights of the syringes to maintain near-stagnant flow. The cells were allowed to adhere within 2 - 4 hours before slightly raising the media syringe to supply fresh media to the channels, and then left to proliferate overnight. On the next day, the chip and syringe apparatus was transferred to the microscope under a temperature and CO₂ environmental chamber as described previously¹⁵. The bacterial culture was then prepared and loaded as described above before imaging. If flow rate was too high, it was lowered when the bacterial population reached the quorum threshold (indicated by the appearance of sfGFP) to allow for better diffusion of the released therapeutic into the mammalian growth channel. For a schematic of the main steps involved, refer to Extended Data Fig. 2d.

For microscopy we used the same system as described in our previous work⁶. Briefly, we used a Nikon Eclipse TI epifluorescent microscope with phase-contrast based imaging. For the acquisition of images, we used a CoolSNAP HQ2 CCD camera from Photometrics. The microscope and acquisition was controlled by the Nikon Elements software. A plexiglass incubation chamber connected to a heating unit, which encompassed a wide area around the stage, was used in order to maintain the temperature of the microfluidic device. Phase-contrast images were taken at 60x magnification at 50-200ms exposure times. Fluorescent imaging at 60x was performed at 150ms for GFP, 30% setting on the Lumencor SOLA light source. Images were taken every 2 - 3 minutes for the course of a typical experiment. In order to estimate the flow rate in the device channel, we measured the length of traces of fluorescent beads (1.0 μm) upon 200ms exposure of fluorescent light to estimate the average fluid velocity. Further information on the analysis of these images is presented in the Data Analysis section below.

Well-plate Experiments

For the viability experiments, we seeded a monolayer of HeLa cells on standard tissue culture 96-well flat bottom plates (Fisher Scientific) with penicillin and streptomycin antibiotics. We grew the four bacterial strains from Fig. 3d in 50 mL cultures to an optical density of 0.08 before pelleting and re-suspending in 1.2 mL media with the appropriate antibiotics. The bacterial cultures were then grown for one hour and then pelleted in a 1.5 mL micro-centrifuge tube. 100 μL of each resulting supernatant was then added to three HeLa culture wells. Thereafter we implemented the protocol for the Vybrant MTT Cell Proliferation Assay Kit (V-13154, Molecular Probes) to measure HeLa cell viability.

For the variable seeding experiments (Fig. 3e-f), we also utilized the same well-plates. We grew the SLC + HlyE strain to an optical density of ~ 0.07 before pelleting the cells and re-suspending in 1 mL of fresh media and antibiotics. Variable volumes of this dense culture were then seeded to three wells for each respective case, and imaging was performed at 20X magnification.

Data Analysis

Fluorescence intensity profiles were obtained by analyzing frames from the fluorescent channel and plotting the mean pixel intensity over time. The period measured is the peak-to-peak period of the fluorescence profile. The number of cells in the trap was found by analyzing the phase-contrast images in ImageJ. Since bacteria formed a monolayer in the growth chamber, we first estimated the average area of an individual bacterial cell and the average void fraction (open space between bacteria in the trap). Taking into account the $\mu\text{m}/\text{pixels}$ of the image, we measured the area of the trap taken up by cells using ImageJ and divided by the average area of a bacterial cell. This value was then multiplied by (1 - void fraction) to yield the total estimated number of cells in the trap. Bacteria that were not close to the main group of cells were counted individually and added to the final number. The fraction of cells lysed per period was estimated by dividing the number of lysed bacteria by the maximum number of bacteria before lysis. Plots were generated by using MATLAB.

In order to estimate the flowrate in the media channel, we imaged fluorescent $1 \mu\text{m}$ beads at 20X and analyzed the images using MATLAB. The length of the fluorescent bead traces was measured in pixels and converted to microns. The length of the trace was then divided by the exposure time (200 ms) to yield the flow velocity. In this study we report the median flow velocity because it is less sensitive to outliers in the bead traces.

Modeling

To describe the dynamic behavior of the SLC we developed an ordinary differential equation model where the populations dynamics track the intracellular concentrations of the variables LuxI (I) and the lysis protein E (L). The population variables are cell population number (N) and extra-cellular AHL (H) (we assume LuxR-AHL binding is fast). This model can be thought of as a system where we follow a surviving lineage (via a single cell) throughout the experiment which responds to extracellular AHL, which in turn increases with cell number. Once the extracellular AHL threshold is reached, the intracellular production of the Lux driven genes, LuxI and E, are brought to the ON state (second stable state), due to the positive feedback provided by the activation term P_{lux} . Increase in the lysis protein leads to a rapid reduction of cell number via the killing term, γ_N , modeled as a hill function to switch killing ON/OFF based on the concentration of lysis protein. Once AHL and lysis protein levels decay, P_{lux} and γ_N turn back to their OFF stable states, allowing cell number to rise and repeat the process. Since firing is dependent on a threshold value of AHL, the SLC can be thought of as a circuit displaying integrate-and-fire behavior.

Maximum cell population (N_0) is defined by the maximum number of cells that could fit inside a single cell trap. Cells leave the trap as the consequence of cell growth (μ_G). The rate of cell degradation through lysis is described by hill function γ_N . We assumed AHL diffusion through the cell membrane to be fast, allowing for dynamic description of total AHL (H) in the trap. Production of AHL (H) is proportional to the product of cell population (N) and per-cell concentration of LuxI (I). AHL dilution is taken to be inversely proportional to N due to the increased blockage of AHL clearance from the trap as the result of cell accumulation. Internal production of LuxI and lysis proteins is described by P_{lux} . Degradation of both proteins is due to cell growth (μ_G) as well

as some basal degradation (γ_I and γ_L). In addition, LuxI is further degraded by ClpXP machinery (γ_C). ClpXP-mediated degradation is used as a proxy for temperature since it is affected by changes in temperature¹⁶.

$$\frac{dN}{dt} = \mu_G N(N_0 - N) - \gamma_N N \quad (1)$$

$$\frac{dH}{dt} = bNI - \frac{\mu H}{1 + N/N_0} \quad (2)$$

$$\frac{dL}{dt} = C_L P_{lux} - \gamma_L L - \mu_G L \quad (3)$$

$$\frac{dI}{dt} = C_I P_{lux} - \gamma_I I - \mu_G I - \gamma_C I \quad (4)$$

$$P_{lux} = \alpha_0 + \frac{\alpha_H (H/H_0)^4}{1 + (H/H_0)^4}$$

$$\gamma_N = \frac{kL^n}{L_0^n + L^n}$$

Parameters:

We chose model parameters to qualitatively fit the experimental population and GFP (proxy for LuxI) trajectories (Fig 2a). Increased protein production and degradation in *S. typhimurium* as compared to *E. coli* was reported in previous work¹⁷. We find that the production and degradation terms in our model (E, LuxI production and basal degradation rates: C_L , C_I , γ_L , γ_I) account for the qualitative differences in behavior between *E. coli* and *S. typhimurium* (Fig. 2b).

Model parameter values:

μ_G (Dilution due to cell growth) 0.2; N_0 (Maximum cell population size) 10; k (Maximum rate of cell lysis) 10; L_0 (Conc. of lysis gene resulting in half maximum lysis) 2; n (Hill coefficient of lysis function) 2; b (AHL production rate) 25; μ (Maximum AHL clearance rate due to flow) 12; C_L (Lysis gene copy number) 0.5; C_I (LuxI copy number) 1; α_0 (Lux promoter basal production) 0.5;

α_H (Lux promoter AHL induced production) 35; H_0 (AHL binding affinity to Lux promoter) 5; γ_L (Basal degradation of lysis protein) 2; γ_I (Basal degradation of LuxI) 2; γ_C (ClpXP degradation of LuxI) 12.

1. Meighen, E. A. Genetics of bacterial bioluminescence. *Annual review of genetics* **28**, 117–139 (1994).
2. Stecher, B. *et al.* Flagella and chemotaxis are required for efficient induction of *Salmonella enterica* serovar typhimurium colitis in streptomycin-pretreated mice. *Infection and immunity* **72**, 4138–4150 (2004).
3. Hohmann, E. L., Oletta, C. A. & Miller, S. I. Evaluation of a phop/phoq-deleted, aroa-deleted live oral *Salmonella typhi* vaccine strain in human volunteers. *Vaccine* **14**, 19–24 (1996).
4. Danino, T., Lo, J., Prindle, A., Hasty, J. & Bhatia, S. N. In vivo gene expression dynamics of tumor-targeted bacteria. *ACS synthetic biology* **1**, 465–470 (2012).
5. Riedel, C. U. *et al.* Construction of p16slux, a novel vector for improved bioluminescent labeling of gram-negative bacteria. *Applied and environmental microbiology* **73**, 7092–7095 (2007).
6. Prindle, A. *et al.* A sensing array of radically coupled genetic ‘biopixels’. *Nature* **481**, 39–44 (2012).
7. Pédelacq, J.-D., Cabantous, S., Tran, T., Terwilliger, T. C. & Waldo, G. S. Engineering and characterization of a superfolder green fluorescent protein. *Nature biotechnology* **24**, 79–88 (2005).

8. Quan, J. & Tian, J. Circular polymerase extension cloning of complex gene libraries and pathways. *PloS one* **4**, e6441 (2009).
9. Lutz, R. & Bujard, H. Independent and tight regulation of transcriptional units in escherichia coli via the lacr/o, the tetr/o and arac/i1-i2 regulatory elements. *Nucleic acids research* **25**, 1203–1210 (1997).
10. Marguet, P., Tanouchi, Y., Spitz, E., Smith, C. & You, L. Oscillations by minimal bacterial suicide circuits reveal hidden facets of host-circuit physiology. *PloS one* **5**, e11909 (2010).
11. Gerdes, K. The parB (hok/sok) locus of plasmid R1: a general purpose plasmid stabilization system. *Nature Biotechnology* **6**, 1402–1405 (1988).
12. Wood, T., Kuhn, R. & Peretti, S. Enhanced plasmid stability through post-segregational killing of plasmid-free cells. *Biotechnology techniques* **4**, 39–44 (1990).
13. Danino, T., Mondragón-Palomino, O., Tsimring, L. & Hasty, J. A synchronized quorum of genetic clocks. *Nature* **463**, 326–330 (2010).
14. Ferry, M., Razinkov, I. & Hasty, J. Microfluidics for synthetic biology from design to execution. *Methods Enzymol* **497**, 295 (2011).
15. Kolnik, M., Tsimring, L. S. & Hasty, J. Vacuum-assisted cell loading enables shear-free mammalian microfluidic culture. *Lab on a chip* **12**, 4732–4737 (2012).
16. Purcell, O., Grierson, C. S., Bernardo, M. & Savery, N. J. Temperature dependence of ssra-tag mediated protein degradation. *Journal of biological engineering* **6**, 10 (2012).
17. Prindle, A. *et al.* Genetic circuits in Salmonella typhimurium. *ACS synthetic biology* **1**, 458–464 (2012).